Materials Science & Engineering A 642 (2015) 391–397

Contents lists available at ScienceDirect

Materials Science & Engineering A

journal homepage: www.elsevier.com/locate/msea

Comparison of crack resistance between ternary CrSiC and quaternary CrSiCN coatings via nanoindentation

Qianzhi Wang [a], Zhiwei Wu [b,c], Fei Zhou [b,c,*], Jiwang Yan [a,**]

[a] Department of Mechanical Engineering, Faculty of Science and Technology, Keio University, Yokohama 2238522, Japan
[b] College of Mechanical and Electrical Engineering, Nanjing University of Aeronautics and Astronautics, Nanjing 210016, China
[c] Jiangsu Key Laboratory of Precision and Micro-Manufacturing Technology, Nanjing 210016, China

ARTICLE INFO

Article history:
Received 3 June 2015
Accepted 9 July 2015
Available online 10 July 2015

Keywords:
PVD coatings
Nanoindentation
Crack
Residual stress
Morphology

ABSTRACT

Quaternary CrSiCN and ternary CrSiC coatings with various Si concentrations were synthesized on Si (100) wafers via adjusting the flow of $(CH_3)_3SiH$ (TMS) in precursor gases. The mechanical property and crack resistance of these coatings were evaluated and compared, as well as the influence of Si concentration was investigated. Compared with the CrSiC coatings, the CrSiCN coatings had higher elasticity and compressive stresses, and in turn, exhibited higher resistance to radial cracks in despite of the Si concentration. The greater thickness of CrSiCN coatings is, the better the crack resistance is. By increasing Si concentration, the compressive stress was released in both categories of coatings, but the trends of crack generation for the two categories of coatings were totally different. For the CrSiCN coatings, a reduction of compressive stress prevented parallel crack initiation around the impression edge after unloading. In contrast, as the compressive stress in the CrSiC coatings was released, radial cracks were generated at the impression corners and the length of radial crack increases with the stress release.

1. Introduction

Silicon nitride (SiN_x) is a promising material for wear protection coatings due to its excellent strength and hardness, low thermal expansion, and durability [1–4]. Thereby, in order to meet growing requirement in industry for superior coatings with good mechanical and tribological properties, academic circles have concentrated on building a composite architecture of nano-crystal dispersing into amorphous SiN_x matrix [5–28]. One of the most common ways is to introduce Si element into transition metal-based coatings such as TiN [6–12], CrN [13–19], ZrN [20], MoN [21], TaN [22], TiCN [23–25] and CrCN [26–28]. For instance, TiSiN coatings presented high hardness over 30 GPa due to refined grain, compact microstructure and a nano-composite architecture after Si addition [9–11]. As a result, long service life was obtained when TiSiN coatings were applied on cutting tools [6,7]. Likewise, with Si alloying, CrSiN coatings became harder than CrN coatings [13–16], and therefore, the friction coefficient and wear rate of tribopair decreased from 0.55 to 0.4 and from 11.0×10^{-7} mm^3/Nm to 5.0×10^{-7} mm^3/Nm, respectively [19]. All the above-mentioned literature indicates that amorphous SiN_x in ternary TiSiN and CrSiN coatings plays an extremely important role in enhancing their mechanical and tribological properties.

As we know, TiCN and CrCN coatings, as potential candidates for TiN and CrN coatings, have attracted researchers' attention for many years due to a combination of hard phase of TiN(CrC) and self-lubrication effect of carbon. However, Fuentes et al. [29] and Warcholinski's group [30–33] pointed out that the residual stress of CrCN coatings was more intensive than CrN coatings, as well as rougher surface. On the other hand, higher density of surface particle, more defects and worse adhesion of TiCN coatings after C doping were reported in Refs. [34,35]. Thus, Si element, which shows positive effect on improving mechanical properties of TiN and CrN coatings, draws researchers' focus again. Kuptsov et al. [23] pointed out that the hardness of TiSiCN coatings increased to 42.9 GPa with 12 at% Si addition, and presented superior impact resistance. In addition, the surface refinement of CrCN coatings by doping Si were reported in Refs. [26,27]. However, previous investigations either studied corrosion behavior alone [26,27], or focused on a specific Si concentration [23,36,37]. So far, there is no systematic research to compare CrSiC with CrSiCN to investigate the advantage of N alloying, as well as the influence of Si concentration on the residual stress, mechanical property and crack resistance of these coatings.

In this study, the microstructure, residual stress, mechanical property and crack resistance of CrSiC and CrSiCN coatings with various Si concentrations were investigated by using X-ray

* Corresponding author. Tel/fax.: +86 25 8489 3083.
** Corresponding author. Tel.: +81 45 566 1445; fax: +81 45 566 1495.
E-mail addresses: fzhou@nuaa.edu.cn (F. Zhou), yan@mech.keio.ac.jp (J. Yan).

http://dx.doi.org/10.1016/j.msea.2015.07.024
0921-5093/

diffraction (XRD), white-light interferometer, nanoindentation and field-emission scanning electron microscope (FE-SEM). Through a comparison of the experimental results, the correlation among the microstructure, the mechanical property and the crack resistance of the coatings was elucidated.

2. Experimental details

2.1. Fabrication of coatings

By using closed-field unbalanced magnetron sputtering system (UDP-650, Teer Coatings Limited, UK), ternary CrSiC and quaternary CrSiCN coatings were fabricated on Si(100) wafers, which were fixed on turning holder after ultrasonic bath in ethanol and deionized water. Prior to deposition, a 30 min. Ar^+ bombardment at bias voltage of −450 V was performed to remove contamination from substrate. After this process, a Cr interlayer with thickness of 0.4 μm was deposited on Si wafer beforehand to enhance the adhesion between substrate and top coating. Subsequently, CrSiC coatings were fabricated by sputtering one Cr target (4.0 A) and one C target (1.0 A) in precursor gases (TMS and Ar). CrSiCN coatings were fabricated by sputtering one Cr target (4.0 A) in precursor gases (TMS, N_2 and Ar). During deposition, the rotating speed of holder, bias voltage and OEM were set as 10 rpm, −80 V and 50%, respectively. Via adjusting the flow of TMS from 10 sccm to 30 sccm, CrSiC and CrSiCN coatings with various Si concentrations were obtained. The symbols of CrSiC(10), CrSiC(20), CrSiC (30), CrSiCN(10), CrSiCN(20) and CrSiCN(30) will be cited to denote coatings deposited under different TMS flows in the next sections.

Table 1
Thickness and element concentration of CrSiCN and CrSiC coatings at different TMS flows.

Coatings	Thickness (μm)	Cr (at%)	Si (at%)	C (at%)	N (at%)
CrSiCN(10)	2.23	40.02	2.67	10.68	46.63
CrSiCN(20)	2.10	47.76	5.53	14.98	31.73
CrSiCN(30)	2.61	49.83	9.86	17.12	23.19
CrSiC(10)	1.79	73.13	1.96	24.91	–
CrSiC(20)	1.80	68.75	3.46	27.79	–
CrSiC(30)	1.71	66.07	7.38	26.55	–

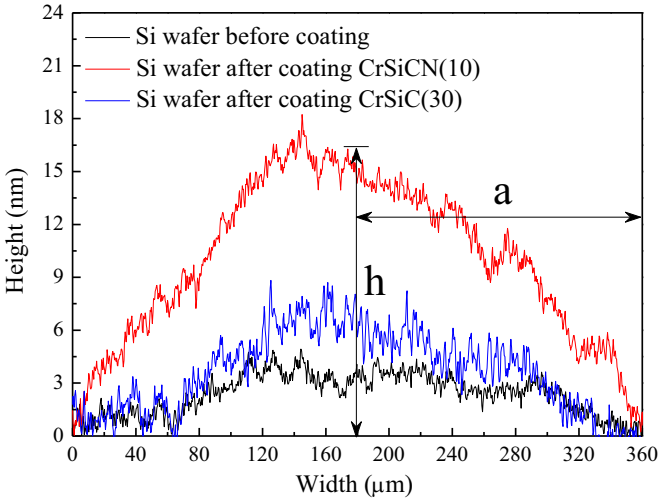

Fig. 1. Cross-section profiles of Si wafers before and after coating CrSiCN(10) and CrSiC(30).

2.2. Phase and residual stress of coatings

The thickness and element concentration of coatings were measured by field emission scanning electron microscope (FE-SEM) (JEOL-JSM-7001F and FEI-SIRION 200), and the results are listed in Table 1. The crystal structure of coatings was characterized by X-ray diffraction spectrum (D8-Advance, Bruker, Germany) with Cu Kα radiation (λ=0.15404 nm) at input voltage (40 kV) and current (40 mA). 2θ data was recorded from 30° to 80° with sampling pitch of 0.01 and scan rate of 10°/min. The cross-section profiles of Si wafers before and after coating, as well as roughness (Gaussian filter, 0.08 mm), were measured by white-light interferometer (CCI 3D, Taylor Hobson Ltd. UK). In here, only contours of CrSiCN(10) and CrSiC(30) coatings are illustrated in Fig. 1 to present the upward bending phenomenon, which is a typical result caused by compressive stress (σ). After the height (h) and width ($2a$) of each contour were measured, individual compressive stress (σ) of coatings could be calculated by Stoney's equation, which has been described in Ref. [38].

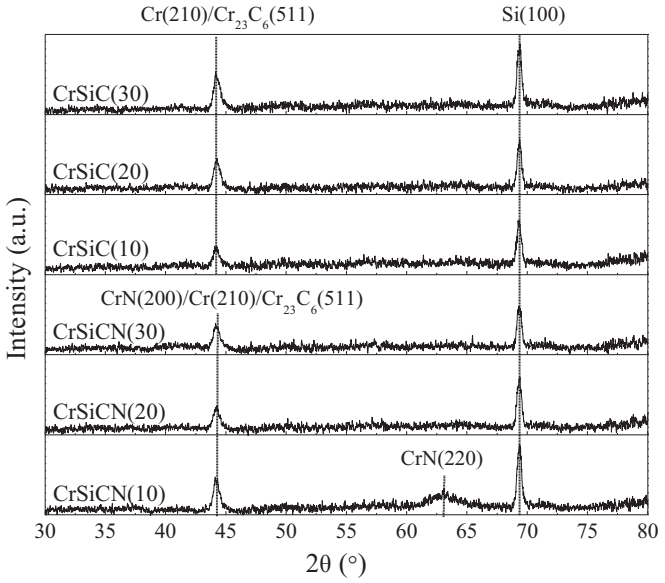

Fig. 2. X-ray diffraction spectra of CrSiCN and CrSiC coatings at different TMS flows.

Table 2
Mechanical properties of CrSiCN and CrSiC coatings at different TMS flows.

Coatings	H (GPa)	SD_H (GPa)	E (GPa)	SD_E (GPa)	H/E	H^3/E^2 (GPa)	W_e (%)	σ (GPa)	d/h
CrSiCN(10)	19.1	2.96	301	31.0	0.063	0.077	55.96	−4.67	0.81
CrSiCN(20)	13.1	0.87	251	11.5	0.052	0.036	47.41	−2.57	0.88
CrSiCN(30)	13.1	0.40	231	6.1	0.057	0.042	48.69	−1.52	0.70
CrSiC(10)	13.8	0.80	271	10.5	0.051	0.036	42.66	−1.71	1.00
CrSiC(20)	13.2	0.64	271	10.6	0.049	0.031	43.49	−1.64	1.00
CrSiC(30)	13.6	1.67	262	19.4	0.052	0.037	44.41	−1.18	1.05

2.3. Mechanical characterization and crack resistance of coatings

The hardness and elastic modulus of the coatings were evaluated by nanoindentation (ENT-1100a, Elionix Co. Ltd.) with Berkovich indenter made of single crystal diamond. A depth of 100 nm was set up to minimize the substrate effect, and 36 nanoindentations were carried out to ensure the reliability of data. Subsequently, the average hardness, elastic modulus with respective deviation standards, H/E, H^3/E^2 as well as elastic recovery were calculated, and these results are listed in Table 2.

At last, 1000 mN was loaded on each coating to verify individual crack resistance. The morphology of impression after high load nanoindentation was observed by field-emission scanning electron microscope (JEOL-JSM-7001F, Japan) to analyze the crack distribution of coatings.

3. Results and discussions

3.1. Element concentration and phase condition of coatings

Because of the additional sputtering of C target during CrSiC coatings deposition, the concentration of C in CrSiC coatings is higher than that in CrSiCN coatings by 10 at% at least. For both of the CrSiC and CrSiCN coatings, the concentration of Si increases gradually with increasing flow of TMS in precursor. Namely, the content of Si increases from 2.67 at% to 9.86 at% in CrSiCN coatings while that raises from 1.96 at% to 7.38 at% in CrSiC coatings. In the same manner, the concentrations of Cr and C in CrSiCN coatings also increase, but the opposite variation trend is obtained for Cr and C elements in CrSiC coatings.

As seen in Fig. 2, besides a sharp diffraction peak around 44̊, a shoulder peak around 63̊ related to CrN(220) exhibits in XRD spectrum of CrSiCN(10) coating. But with more Si incorporation, the XRD spectra of CrSiCN(20) and CrSiCN(30) coatings only

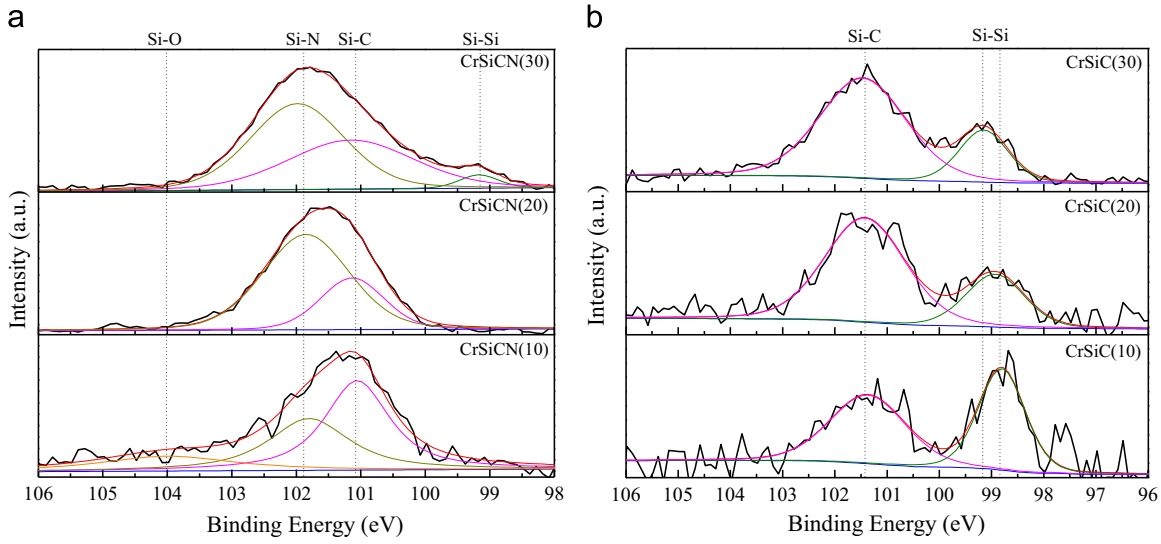

Fig. 3. Si_{2p} XPS of (a) CrSiCN and (b) CrSiC coatings at different TMS flows.

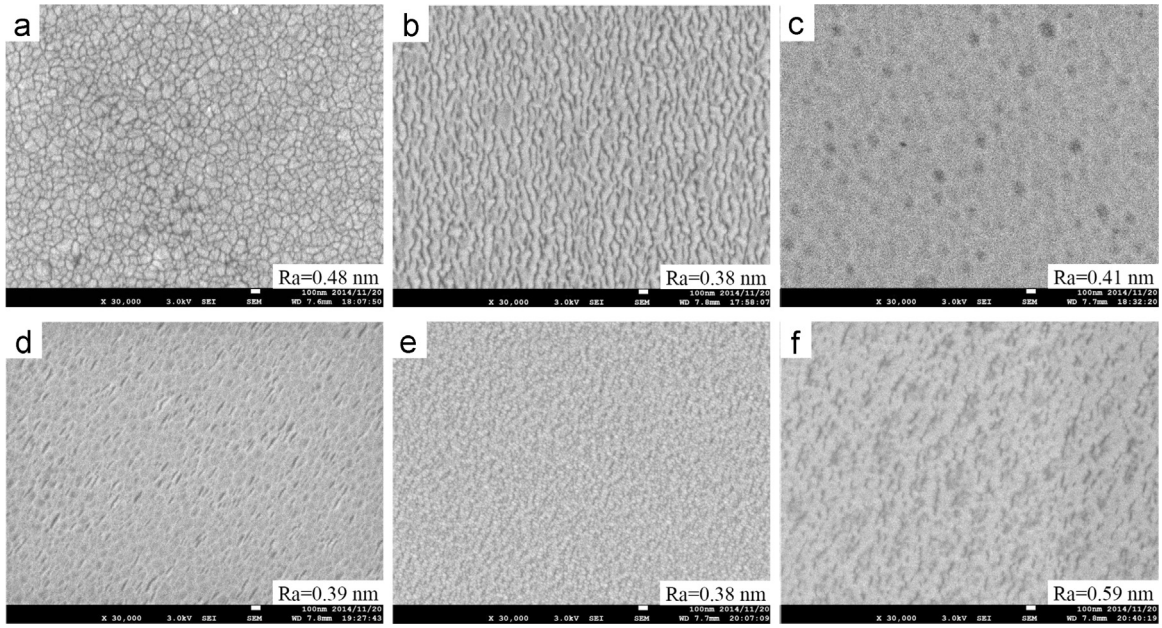

Fig. 4. SEM images of morphology of (a) CrSiCN(10) (b) CrSiCN(20) (c) CrSiCN(30) (d) CrSiC(10) (e) CrSiC(20) (f) CrSiC(30) coatings.

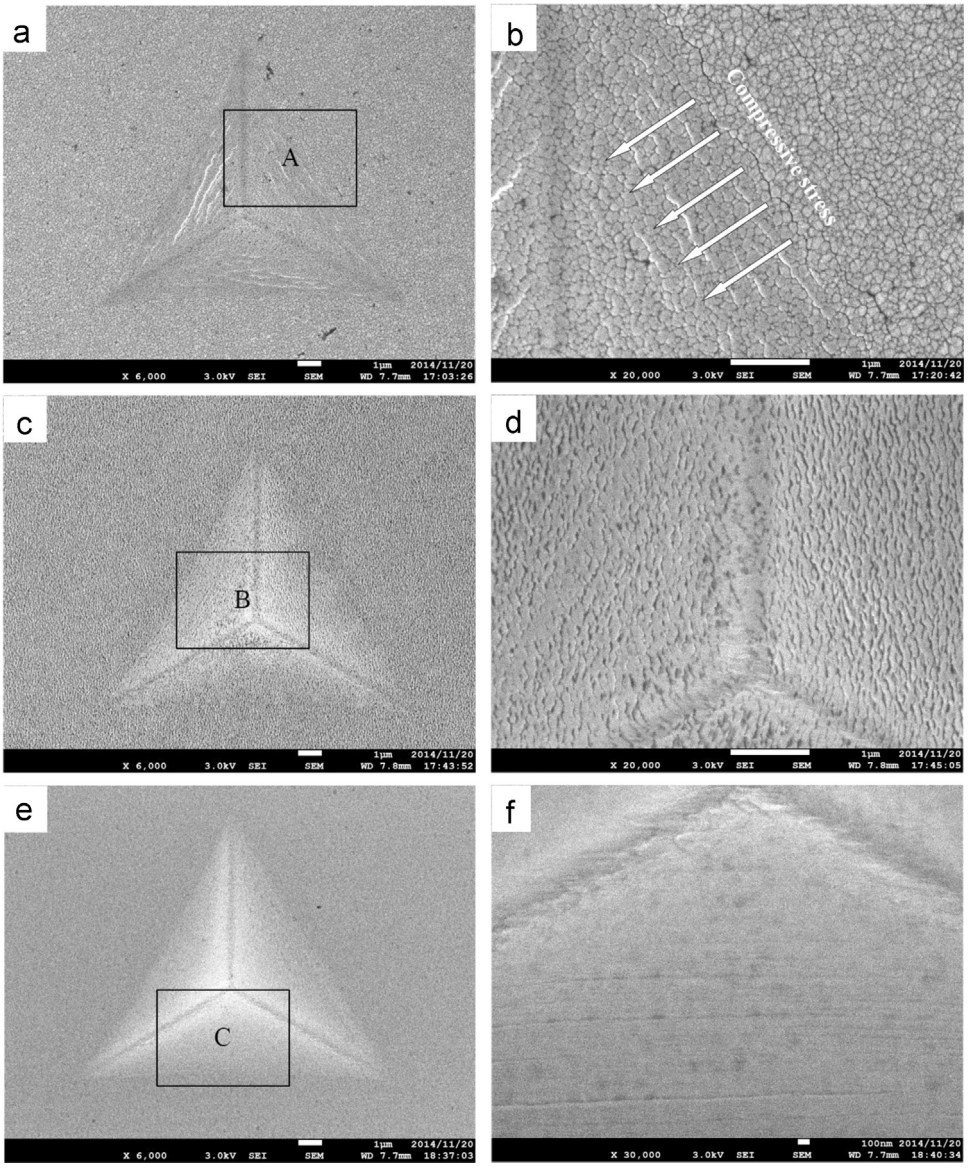

Fig. 5. SEM images of nanoindentations of (a) CrSiCN(10) (b) Area A of CrSiCN(10) (c) CrSiCN(20) (d) Area B of CrSiCN(20) (e) CrSiCN(30) (f) Area C of CrSiCN(30).

present a preferred diffraction peak around 44̊, which is related to CrN(200), $Cr_{23}C_6$(511) and adhesive layer Cr(210) simultaneously (JCPDS 11-0065, JCPDS 19-0323 and JCPDS 35-0783). It is indicated that more Si alloying can inhibit the growth of CrN(220) in CrSiCN coatings, and the similar result was reported in Ref. [28]. With regard to ternary CrSiC coatings, no matter how much Si was incorporated, only a preferred diffraction peak around 44̊ related to $Cr_{23}C_6$(511) and adhesive layer Cr(210) appears. It is worth noting that no diffraction peaks of SiC and Si_3N_4 crystals were detected in XRD spectra. Thus, the silicon in CrSiC and CrSiCN coatings should exist in terms of amorphous SiC_x and SiN_x, which has been covered by other research groups [24–28].

In order to prove the presence of SiC_x and SiN_x, Si_{2p} fractal X-ray photoelectron spectra of CrSiC and CrSiCN are illustrated in Fig. 3. Obviously, the main peak of all the CrSiCN coatings could be deconvoluted into two overlapped peaks related to Si–C bond around 101.1 eV and Si–N bond around 101.8 eV [24,39–41]. Moreover, the volume fraction of Si–N bond increases with increasing Si concentration, and finally a novel and weak Si–Si bond presents at 99.2 eV due to higher Si incorporation in CrSiCN(30) coating. On the other hand, only Si–C bond at 101.2 ± 0.2 eV accompanying with Si–Si bond at 99.0 ± 0.2 eV exhibits in Si_{2p} fractal X-ray photoelectron spectra of CrSiC coatings [42]. Moreover, with increasing concentration of Si in CrSiC coatings, the volume fraction of Si–C bond rises while that of Si–Si bond drops. Thus, taking into account the results of XRD and XPS, Si element exists in CrSiCN and CrSiC coatings as amorphous SiN_x and SiC_x.

3.2. Mechanical properties of coatings

The mechanical properties and residual stress extracted from nanoindentation and cross-section profiles of Si wafers are listed in Table 2. It is clear that the hardness of CrSiC coatings with different Si contents varies slightly in a range of 13.2–13.8 GPa, but the standard deviation of hardness (SD_H) increases sharply from 0.64 GPa to 1.67 GPa when the Si concentration raises from 3.46 at% to 7.38 at%. In contrast, SD_H of CrSiCN coatings decreases continuously from 2.96 GPa to 0.4 GPa with increasing Si concentration, and the hardness drops from 19.1 GPa for CrSiCN(10) to 13.1 GPa for CrSiCN(20) and CrSiCN(30). Generally, hardness is closely related to microstructure or phase condition of coatings while SD_H depends on their compactness strongly. Thus, the close

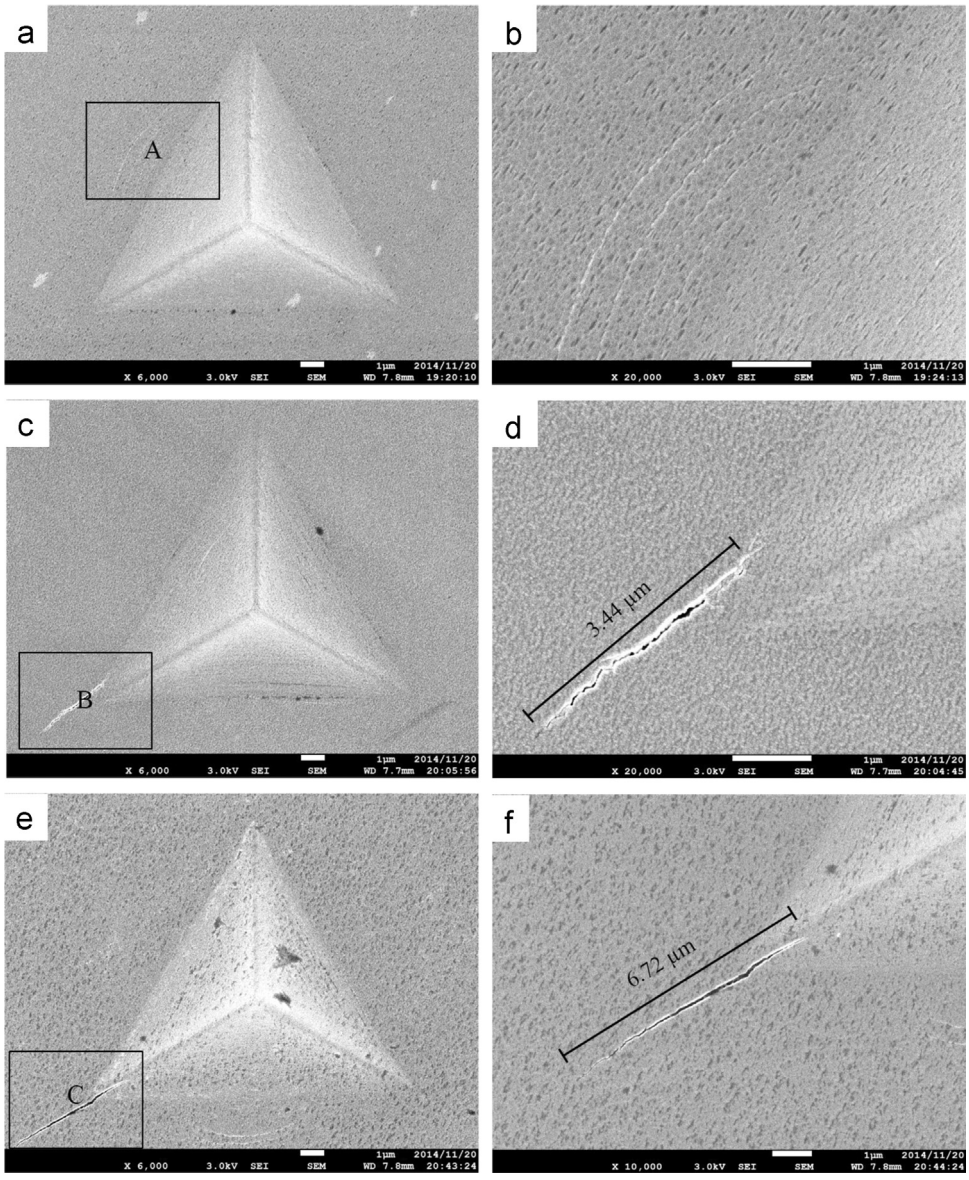

Fig. 6. SEM images of nanoindentations of (a) CrSiC(10) (b) Area A of CrSiC(10) (c) CrSiC(20) (d) Area B of CrSiC(20) (e) CrSiC(30) (f) Area C of CrSiC(30).

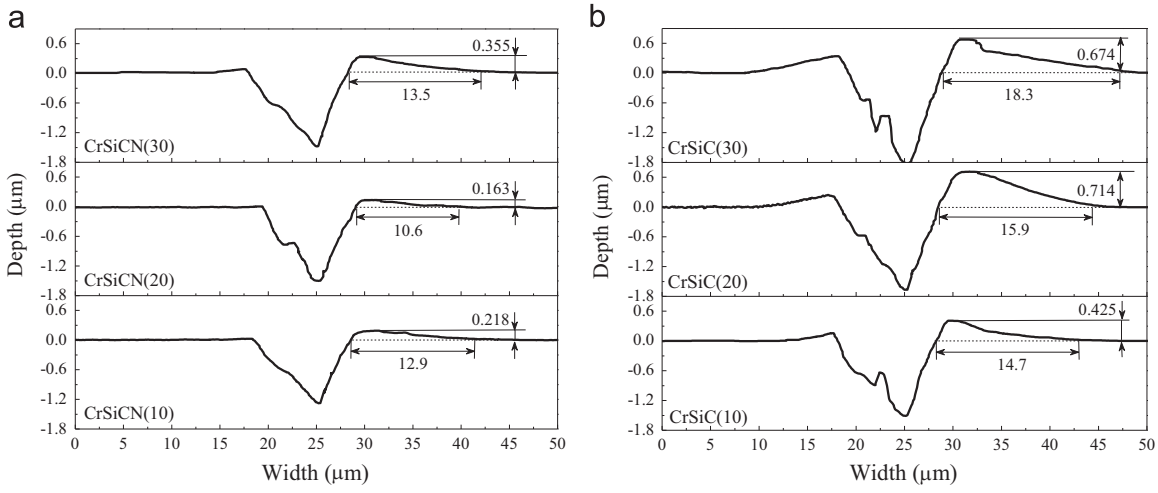

Fig. 7. Contours of nanoindentations of (a) CrSiCN and (b) CrSiC coatings at different TMS flows.

resemblance in XRD spectra of CrSiC(10), CrSiC(20), CrSiC(30), CrSiCN(20) and CrSiCN(30) coatings, i.e. their similar microstructure maintains the hardness in a small range of 13.1 GPa to 13.8 GPa, while CrSiCN(10) coating with two diffraction peaks presents the highest hardness of 19.1 GPa. On the other hand, the obvious boundary of column structure shown in Fig. 4a is a main factor contributing to highest SD_H of CrSiCN(10) coating, because the tip of indenter happens to penetrate into these boundaries. The relatively higher roughness of CrSiCN(10) and CrSiC(30) coatings also results in their higher SD_H. In addition, the seamless morphology of coatings without obvious crystal boundary in Fig. 4b–f is another proof of formation of amorphous phase. Also, this is an additional reason why CrSiC(10), CrSiC(20), CrSiC(30), CrSiCN(20) and CrSiCN(30) coatings present lower hardness, because the amorphous phase state is the lower limit of the nanocrystalline state [43].

Generally, the H/E reflects elastic strain to failure whilst H^3/E^2 is proportional to plastic deformation resistance to a certain extent [44]. Here, all of the CrSiCN coatings present higher H/E and H^3/E^2 than those of all the CrSiC coatings as listed in Table 2, and this indicates that CrSiCN coatings may possess superior crack resistance to CrSiC coatings. From another point of view, the variation of elastic recovery (W_e) extracted from load-unload curve is well consistent with the changing trend of H/E and H^3/E^2. In other word, all of the CrSiCN coatings also exhibit a higher W_e than all of the CrSiC coatings. Pettersson et al. [45] investigated the mechanical properties of SiN_x and SiC_xN_y coatings, and found that the H/E of SiN_x coatings reduced after introducing C into SiN_x coatings due to the formation of SiC_x with high elastic modulus. Statistically, Si_3N_4 generally exhibits the lower elastic modulus as compared with SiC [46]. Thus, the reason to the higher H/E and H^3/E^2 of CrSiCN coatings is the presence of SiN_x that lowers the elastic modulus. With regard to the compressive stress ($\sigma < 0$), the Si in CrSiCN and CrSiC coatings presents the same effect that the compressive stress is released by more Si addition due to the more formation of amorphous SiC_x and SiN_x [15,38].

3.3. Crack resistance of coatings

The nanoindentation impressions of CrSiCN and CrSiC coatings under a maximum indentation load of 1000 mN are illustrated in Fig. 5 and Fig. 6, respectively. As seen in Fig. 5a, c and e, no radial crack presents at impression corners of CrSiCN coatings no matter how much Si was incorporated. Instead, there are a few pile-up steps near the impression edge of CrSiC(10) coating in Fig. 6b; while the CrSiC(20) and CrSiC(30) coatings have obvious radial cracks, as shown in Fig. 6d and f. Generally, there are three contributors to the crack resistance of coatings: (1) Mechanical property of the substrate; (2) Microstructure, compactness and mechanical property of coatings; (3) Residual stress (σ_c) after deposition [47,48]. Since all of the coatings in this study were deposited on Si(100) wafer, the effect of substrate property is minimized. In other word, the second and the third factors should be the main reasons to determine crack resistance of coatings here. As above-mentioned, the CrSiCN coatings should exhibit superior crack inhibition effect due to higher H/E, H^3/E^2 and elastic recovery, and therefore, no radial crack forms during loading process. In contrast, the CrSiC(10), CrSiC(20) and CrSiC(30) coatings with relatively low H/E, H^3/E^2 and elastic recovery encounter pile-up and radial crack during loading process. On the other hand, the ratio of penetration depth to coatings thickness (d/h) also determines the crack resistance to a certain extent. At large, penetration depth close to or even over the thickness of coatings makes the radial crack occur easily [48]. Thus, the higher d/h of CrSiC leads to occurrence of radial cracks too.

However, it is worth noting that there are some tiny cracks parallel to the impression edge of CrSiCN(10) coating (Fig. 5b). This phenomenon might be caused by the highest compressive stress (4.67 GPa). During loading process, radial crack was inhibited in a degree under the effect of compressive stress. But after unloading, the balance of initial compressive stress along the impression edge was broken, the compressive stress stretched the coating towards the impression center. Thus, the CrSiCN(10) coatings with less compactness is easy to be peeled off [38]. Another difference is that there is no radial crack, but pile-up forms on the impression of CrSiC(10) coating. Among three kinds of CrSiC coatings, CrSiC (10) coating exhibits the lowest elastic recovery and the highest compressive stress. During loading process, plastic deformation is easy to occur for the CrSiC(10) coating. As a result, it is easy to form pile-ups and to inhibit radial cracks. As the Si concentration in CrSiC coatings increases, the compressive stress decreases accordingly. Thus, the radial crack with a length of 3.44 μm initiates at the corner of impression for CrSiC(20). When the compressive stress keeps on reducing to 1.18 GPa for CrSiC(30) coating, the length of radial crack (6.72 μm) becomes longer.

According to the value of W_e in Table 2, all of CrSiC coatings present lower W_e as compared with CrSiCN coatings. In other words, CrSiC coatings confront plastic deformation more easily than CrSiCN coatings. Subsequently, as seen in Fig. 7, the width and height of pile-up for CrSiC coatings are always higher than those for CrSiCN coatings. Regarding each category, CrSiC(30) and CrSiCN(30) coatings exhibit the lowest compressive stress due to more amorphous SiC_x and SiN_x. Thus, CrSiC(30) and CrSiCN(30) coatings were more difficult to recover after unloading as compared to the rest coatings with higher compressive stress. This is the reason why CrSiC(30) and CrSiCN(30) coatings present the highest height and width of pile-up.

4. Conclusions

The mechanical property as well as crack resistance of ternary CrSiC and quaternary CrSiCN coatings with various Si concentrations was investigated via high-load nanoindentation. Conclusions are drawn as follows:

1. Owing to the presence of amorphous SiN_x with lower elastic modulus and higher toughness, all of the quaternary CrSiCN coatings, as compared with the ternary CrSiC coatings, presented superior crack resistance.
2. A thicker CrSiCN coating contributes to the inhibition of crack initiation.
3. Increasing Si concentration released the compressive stress in both CrSiC and CrSiCN coatings. The reduction of compressive stress prevented crack generation parallel to the impressive edge for CrSiCN coatings, but led to radial cracks for CrSiC coatings.
4. The CrSiCN(20) coating with 5.53 at% Si exhibited the highest crack resistance to both parallel cracks and radial cracks due to its optimal combination of mechanical property, compressive stress and elastic recovery.

Acknowledgment

This work has been initiated from a Japan–China joint research project and partially supported by a research grant in Keio University. This work has been also supported by National Natural Science Foundation of China (Grant no. 51375231), Doctoral Program of Higher Education (Grant no. 20133218110030), Priority

Academic Program Development of Jiangsu Higher Education Institutions (PAPD), Jiangsu Innovation Program for Graduate Education (Grant no. KYLX0234) and the Fundamental Research Funds for the Central Universities.

References

[1] K.N. Lee, D.S. Fox, N.P. Bansal, Rare earth silicate environmental barrier coatings for SiC/SiC composites and Si_3N_4 ceramics, J. Eur. Ceram. Soc. 25 (2005) 1705–1715.

[2] J.P. Kim, E.H. Kim, J.H. Lee, Y.G. Jung, N.H. Kim, S.C. Choi, U. Paik, Damage resistance of SiC and Si_3N_4 coatings with control of microstructure and thickness, Prog. Org. Coat. 64 (2009) 274–280.

[3] X.M. Li, X.W. Yin, L.T. Zhang, T.H. Pan, Comparison in microstructure and mechanical properties of porous Si_3N_4 ceramics with SiC and Si_3N_4 coatings, Mater. Sci. Eng. A 527 (2009) 103–109.

[4] M. Pettersson, S. Tkachenko, S. Schmidt, T. Berlind, S. Jacobson, L. Hultman, H. Engqvist, C. Persson, Mechanical and tribological behavior of silicon nitride and silicon carbon nitride coatings for total joint replacements, J. Mech. Behav. Biomed. 25 (2013) 41–47.

[5] Y.X. Wang, S. Zhang, Toward hard yet tough ceramic coatings, Surf. Coat. Technol. 258 (2014) 1–16.

[6] C.T. Guo, D. Lee, P.C. Chen, Deposition of TiSiN coatings by arc ion plating process, Appl. Surf. Sci. 254 (2008) 3130–3136.

[7] I. Camps, S. Muhl, E. Camps, J.G. Quiñones-Galván, M. Flores, Tribological properties of TiSiN thin films deposited by laser ablation, Surf. Coat. Technol. 255 (2014) 74–78.

[8] C.L. Chang, C.T. Lin, P.C. Tsai, W.Y. Ho, D.Y. Wang, Influence of bias voltages on the structure and wear properties of TiSiN coating synthesized by cathodic arc plasma evaporation, Thin Solid Films 516 (2008) 5324–5329.

[9] J. Perez-Mariano, K.H. Lau, A. Sanjurjo, J. Caro, D. Casellas, C. Colominas, TiSiN nanocomposite coatings by chemical vapor deposition in a fluidized bed reactor at atmospheric pressure (AP/FBR-CVD), Surf. Coat. Technol. 201 (2006) 2217–2225.

[10] J. Houska, J.E. Klemberg-Sapieha, L. Martinu, Atomistic simulations of the characteristics of TiSiN nanocomposites of various compositions, Surf. Coat. Technol. 203 (2009) 3348–3355.

[11] K.D. Bouzakis, G. Skordaris, S. Gerardis, G. Katirtzoglou, S. Makrimallakis, M. Pappa, E. Lill, R. MSaoubi, Ambient and elevated temperature properties of TiN, TiAlN and TiSiN PVD films and their impact on the cutting performance of coated carbide tools, Surf. Coat. Technol. 204 (2009) 1061–1065.

[12] P.C. Wo, P.R. Munroe, Z.F. Zhou, K.Y. Li, Z.H. Xie, Effects of TiN sublayers on the response of TiSiN nanocomposite coatings to nanoidentation and scratching contacts, Mater. Sci. Eng. A 527 (2010) 4447–4457.

[13] D. Mercsa, N. Bonasso, S. Naamane, J.M. Bordes, C. Coddet, Mechanical and tribological properties of Cr–N and Cr–Si–N coatings reactively sputter deposited, Surf. Coat. Technol. 200 (2005) 403–407.

[14] S.Y. Lee, B.S. Kim, S.D. Kim, G.S. Kim, Y.S. Hong, Effect of Si doping on the wear properties of CrN coatings synthesized by unbalanced magnetron sputtering, Thin Solid Films 506–507 (2006) 192–196.

[15] P.C. Wo, P.R. Munroe, Z. Li, Z.-T. Jiang, Z.H. Xie, Z.F. Zhou, K.Y. Li, Factors governing the mechanical behaviour of CrSiN coatings: combined nanoindentation testing and transmission electron microscopy, Mater. Sci. Eng. A 534 (2012) 297–308.

[16] M.D. Bao, X.B. Xu, W. Sebastien, H.L. Sun, T. Dennis, J.W. He, Microabrasive wear resistance of CrN and CrSiN coatings, Plasma Process. Polym. 4 (2007) S607–S612.

[17] M. Benkahoul, P. Robin, S.C. Gujrathi, L. Martinu, J.E. Klemberg-Sapieha, Microstructure and mechanical properties of Cr–Si–N coatings prepared by pulsed reactive dual magnetron sputtering, Surf. Coat. Technol. 202 (2008) 3975–3980.

[18] G.G. Zhang, L.P. Wang, S.C. Wang, P.X. Yan, Q.J. Xue, Structure and mechanical properties of reactive sputtering CrSiN films, Appl. Surf. Sci. 255 (2009) 4425–4429.

[19] J.L. Lin, B. Wang, Y.X. Ou, W.D. Sproul, I. Dahan, J.J. Moore, Structure and properties of CrSiN nanocomposite coatings deposited by hybrid modulated pulsed power and pulsed dc magnetron sputtering, Surf. Coat. Technol. 216 (2013) 251–258.

[20] H. Zhang, T.W. Guo, Z.X. Song, X.J. Wang, K.W. Xu, The effect of ZrSiN diffusion barrier on the bonding strength of titanium porcelain, Surf. Coat. Technol. 201 (2007) 5637–5640.

[21] Q. Liu, Q.F. Fang, F.J. Liang, J.X. Wang, J.F. Yang, C. Li, Synthesis and properties of nanocomposite MoSiN hard films, Surf. Coat. Technol. 201 (2006) 1894–1898.

[22] Y.I. Chen, K.Y. Lin, H.H. Wang, K.C. Lin, Thermal stability of TaN, CrTaN, TaSiN, and CrTaSiN hard coatings in oxygen-containing atmospheres, Surf. Coat. Technol. 259 (2014) 159–166.

[23] K.A. Kuptsov, Ph.V. Kiryukhantsev-Korneev, A.N. Sheveyko, D.V. Shtansky, Comparative study of electrochemical and impact wear behavior of TiCN, TiSiCN, TiCrSiCN, and TiAlSiCN coatings, Surf. Coat. Technol. 216 (2013) 273–281.

[24] I. Endler, M. Höhn, J. Schmidt, S. Scholz, M. Herrmann, M. Knaut, Ternary and quarternary TiSiN and TiSiCN nanocomposite coatings obtained by chemical vapor deposition, Surf. Coat. Technol. 215 (2013) 133–140.

[25] H. Xu, X. Nie, R. Wei, Tribological behavior of a TiSiCN coating tested in air and coolant, Surf. Coat. Technol. 201 (2006) 4236–4241.

[26] F. Cai, X. Huang, Q. Yang, R.H. Wei, D. Nagy, Microstructure and tribological properties of CrN and CrSiCN coatings, Surf. Coat. Technol. 205 (2010) 182–188.

[27] F. Cai, Q. Yang, X. Huang, R.H. Wei, Microstructure and corrosion behavior of CrN and CrSiCN coatings, J. Mater. Eng. Perform. 19 (2010) 721–727.

[28] J.H. Jeon, C.S. Jang, S.Y. Yoon, B.C. Shin, K.H. Kim, Effects of Si addition on the characteristic evolution and syntheses of nanocomposite Cr–Si–C–N coatings prepared by a hybrid coating system, Surf. Coat. Technol. 200 (2005) 1635–1639.

[29] G.G. Fuentes, M.J. Díaz de Cerio, J.A. García, R. Martínez, R. Bueno, R. J. Rodríguez, M. Rico, F. Montalá, Y. Qin, Gradient CrCN cathodic arc PVD coatings, Thin Solid Films 517 (2009) 5894–5899.

[30] B. Warcholinski, A. Gilewicz, Z. Kuklinski, P. Myslinski, Hard CrCN/CrN multilayer coatings for tribological applications, Surf. Coat. Technol. 204 (2010) 2289–2293.

[31] B. Warcholinski, A. Gilewicz, Z. Kuklinski, P. Myslinski, Arc-evaporated CrN, CrN and CrCN coatings, Vacuum 83 (2009) 715–718.

[32] B. Warcholinski, A. Gilewicz, Effect of substrate bias voltage on the properties of CrCN and CrN coatings deposited by cathodic arc evaporation, Vacuum 90 (2013) 145–150.

[33] B. Warcholinski, A. Gilewicz, The properties of multilayer CrCN/CrN coatings dependent on their architecture, Plasma Process. Polym. 8 (2011) 333–339.

[34] S.W. Huang, M.W. Ng, M. Samandi, M. Brandt, Tribological behaviour and microstructure of $TiC_xN_{(1-x)}$ coatings deposited by filtered arc, Wear 252 (2002) 566–579.

[35] Y.H. Cheng, T. Browne, B. Heckerman, E.I. Meletis, Influence of the C content on the mechanical and tribological properties of the TiCN coatings deposited by LAFAD technique, Surf. Coat. Technol. 205 (2011) 4024–4029.

[36] Y.J. Zheng, Y.X. Leng, X. Xin, Z.Y. Xu, F.Q. Jiang, R.H. Wei, N. Huang, Evaluation of mechanical properties of Ti(Cr)SiC(O)N coated cemented carbide tools, Vacuum 90 (2013) 50–58.

[37] Q. Li, F.Q. Jiang, Y.X. Leng, R.H. Wei, N. Huang, Microstructure and tribological properties of Ti(Cr)SiCN coating deposited by plasma enhanced magnetron sputtering, Vacuum 89 (2013) 168–173.

[38] Q.Z. Wang, Z.W. Wu, F. Zhou, H. Huang, K. Niitsu, J.W. Yan, Evaluation of crack resistance of CrSiCN coatings as a function of Si concentration via nanoindentation. Surf. Coat. Technol. 272, 2015, 239-245.

[39] M.S. Ahmed, P. Munroe, Z.T. Jiang, X.L. Zhao, W. Rickard, Z.F. Zhou, L.K.Y. Li, Z. H. Xie, Corrosion behaviour of nanocomposite TiSiN coatings on steel substrates, Corros. Sci. 53 (2011) 3678–3687.

[40] A. Vladescu, V. Braic, M. Braic, M. Balaceanu, Arc plasma deposition of TiSiN/Ni nanoscale multilayered coatings, Mater. Chem. Phys. 138 (2013) 500–506.

[41] I. Bertoti, M. Mohai, K. Kereszturi, A. Toth, E. Kalman, Carbon based Si- and Cr-containing thin films: chemical and nanomechanical properties, Solid State Sci. 11 (2009) 1788–1792.

[42] ⟨http://srdata.nist.gov/xps/⟩.

[43] M.A. Meyers, A. Mishra, D.J. Benson, Mechanical properties of nanocrystalline materials, Prog. Mater. Sci. 51 (2006) 427–556.

[44] N.A. Sakharova, J.V. Fernandes, M.C. Oliveira, J.M. Antunes, Influence of ductile interlayers on mechanical behaviour of hard coatings under depth-sensing indentation: a numerical study on TiAlN, J. Mater. Sci. 45 (2010) 3812–3823.

[45] M. Pettersson, S. Tkachenko, S. Schmidt, T. Berlind, S. Jacobson, L. Hultman, H. Engqvist, C. Persson, Mechanical and tribological behavior of silicon nitride and silicon carbon nitride coatings for total joint replacements, J. Mech. Behav. Biomed. 25 (2013) 41–47.

[46] ⟨http://accuratus.com/silicar.html⟩.

[47] M. Jirout, J. Musil, Effect of addition of Cu into ZrO_x film on its properties, Surf. Coat. Technol. 200 (2006) 6792–6800.

[48] J. Musil, M. Jirout, Toughness of hard nanostructured ceramic thin films, Surf. Coat. Technol. 201 (2007) 5148–5152.